A&A, 708, A341 (2026)
https://doi.org/10.1051/0004-6361/202658996
© The Authors 2026

Astronomy & Astrophysics

# Diverse lifestyles of bar-like galaxies and their coevolution with the brightest galaxy in the most massive cluster of TNG50

Ewa L. Łokas*

Nicolaus Copernicus Astronomical Center, Polish Academy of Sciences, Bartycka 18, 00-716 Warsaw, Poland

Received 16 January 2026 / Accepted 11 March 2026

**ABSTRACT**

Clusters can provide propitious environments for bar formation in galaxies. This work studies the formation and evolution of 15 bar-like galaxies in the most massive cluster of the TNG50 simulation from the IllustrisTNG suite. The selection includes galaxies from the last simulation output from well-resolved subhalos with a strongly prolate stellar component. Eleven galaxies form or strongly enhance their bars during a pericenter passage around one or more progenitors of the brightest cluster galaxy (BCG). Two form their bars early as a result of minor mergers, one via an interaction with another massive galaxy, and one via disk instability. The bar formation times differ considerably, ranging between 3–11 Gyr. The lengths of the bars also differ, ranging between 2–6 kpc, and do not correlate with the amount of tidal forcing experienced. All galaxies have at least one pericenter passage around a BCG progenitor, but the number of interactions varies strongly and is reflected in the different amount of mass stripping the galaxies experience. Most bar formation events take place before the BCG is fully formed. In three cases, they occur just before different progenitors of the BCG merge. For six bar-like galaxies, the merger events leading to the final formation of the BCG cause significant changes of their orbits. Their diverse evolutionary histories illustrate the different paths to bar formation in clusters and emphasize the complex nature of the process, which includes coevolution with BCG progenitors.

**Key words.** galaxies: clusters: general – galaxies: evolution – galaxies: interactions – galaxies: kinematics and dynamics – galaxies: spiral – galaxies: structure

## 1. Introduction

Bars in galaxies are generally believed to form as a result of the inherent instability of their disks (Hohl 1971; Ostriker & Peebles 1973; Athanassoula 2003). Recently, however, another possible scenario for their formation has received considerable attention, namely the one involving interactions with other objects. Since interactions occur more frequently at the early stages of galactic evolution, this scenario has been evoked especially in the context of recent discoveries of high-redshift bars with James Webb Space Telescope (JWST) (Guo et al. 2023; Costantin et al. 2023; Amvrosiadis et al. 2025; Łokas 2025a,c) and measurements of nonzero bar fractions at early epochs (Le Conte et al. 2024; Guo et al. 2025; Géron et al. 2025).

Interactions leading to bar formation in disky galaxies can take many forms and can involve dwarf galaxies orbiting a Milky Way-like host (Łokas et al. 2014, 2015; Gajda et al. 2017, 2018), a flyby of an object of similar mass (Noguchi 1987; Gerin et al. 1990; Miwa & Noguchi 1998; Berentzen et al. 2004; Łokas 2018), or a Milky Way-like galaxy orbiting a cluster (Mastropietro et al. 2005; Łokas et al. 2016). In all these configurations, studied mostly through controlled $N$-body simulations, the mechanism of bar formation is the same and related to the tidal force acting on the disk, which distorts it and induces more radial orbits of the stars. The effect is larger for more massive hosts, smaller pericenter distances, and more prograde orientations of the disk with respect to the orbit. Sufficient tidal force leads to a fast transformation of almost the whole stellar component from an oblate to a prolate shape. The resulting shape of the object is bar-like rather than barred, since little of a disk remains in which the bar could be embedded.

The formation of tidal bars in the cluster environment is particularly promising because of the strong tidal force exerted by the brightest cluster galaxy (BCG). Since most cluster members are expected to experience at least one pericenter passage around their BCG, this environment should efficiently produce tidal bars, and we expect an increased fraction of barred galaxies toward the cluster center. Currently, there is no clear observational evidence supporting this relationship, although early studies appeared to support this hypothesis (Thompson 1981; Andersen 1996; Barazza et al. 2009). However, later studies found little or no significant dependence of the bar fraction on the clustercentric distance (Méndez-Abreu et al. 2010; Lansbury et al. 2014; Cervantes Sodi et al. 2015; Łokas et al. 2016) and pointed to other factors as decisive in bar formation and properties, such as the stellar mass, size and morphological type of the galaxy (Tawfeek et al. 2022; Aguerri et al. 2023).

Simulations of galaxy formation and evolution can help clarify the situation. In Łokas et al. (2016), we considered a very idealized configuration in which an $N$-body model of a Milky Way-like galaxy was placed on different orbits in a Virgo-like cluster and evolved for 10 Gyr. The Milky Way galaxy was composed of a disk and a dark matter halo, whereas the Virgo cluster was approximated as a single, preexisting, although live, dark halo. These controlled experiments demonstrate that, in such an environment, bars form much faster than in isolation, particularly on tighter orbits.

Cosmological simulations of galaxy formation, such as IllustrisTNG (Springel et al. 2018; Marinacci et al. 2018; Naiman et al. 2018; Nelson et al. 2018; Pillepich et al. 2018),

* Corresponding author: lokas@camk.edu.pl



Open Access article, published by EDP Sciences, under the terms of the Creative Commons Attribution License (https://creativecommons.org/licenses/by/4.0), which permits unrestricted use, distribution, and reproduction in any medium, provided the original work is properly cited.
This article is published in open access under the Subscribe to Open model. Subscribe to A&A to support open access publication.

provide an ideal tool to place this scenario in a more realistic context. These simulations follow the evolution of both dark matter and the baryonic component in boxes of different size and resolution (TNG50, TNG100, and TNG300) by solving for gravity and magnetohydrodynamics and are supplemented by subgrid prescriptions for processes such as star formation, stellar feedback, and black hole feedback. In such simulations, the bars are formed alongside other phenomena, such as galaxy clustering into groups and BCG formation via mergers of massive galaxies, which complicates the picture compared to the evolution of a single galaxy in a preexisting cluster. In Łokas (2020), I studied the tidal evolution of galaxies in the most massive cluster of TNG100 and showed that bars can indeed form via interactions with a BCG, presenting several examples.

Interesting candidates for tidally induced bars occur among bar-like galaxies. These are not bars embedded in disks, as previously studied using Illustris and IllustrisTNG (Peschken & Łokas 2019; Rosas-Guevara et al. 2020, 2022, 2025; Zhou et al. 2020; Zhao et al. 2020), but rather objects whose overall stellar component can be approximated as a prolate spheroid. In Łokas (2021), I studied a sample of bar-like galaxies in the TNG100 simulation, selected among well-resolved objects (total stellar mass above $10^{10}\,\mathrm{M}_\odot$), with a single condition that the intermediate-to-longest axis ratio $b/a$ of the stellar component (within two stellar half-mass radii, $2r_{1/2}$) be lower than 0.6. The sample contained 277 bar-like galaxies, which could be divided into three classes based on the origin of the bar and the subsequent evolution. In class A galaxies (77 objects, 28% of the sample), an interaction with a larger perturber, typically a central galaxy of a group or cluster, induced the bar. In classes B and C (27% and 45% of the sample, respectively), a minor merger, a small satellite, or disk instability induced the bars. While class B galaxies were partially stripped of mass, those of class C evolved in isolation, retaining their mass content.

Łokas (2025b) provides a detailed study of the 77 bar-like galaxies of class A whose strong bars were induced by an interaction with more massive objects in a cluster. For the entire subsample, the time of bar formation strongly correlated with and was typically slightly greater than the time of the pericenter passage around the host. All galaxies were strongly stripped of dark matter and gas, and their rotation was diminished. Larger pericenter distances typically required higher host masses to transform the galaxies. Despite difficulties in interpreting some cases involving mergers and multiple interactions, the results confirmed, in the cosmological context, the reality of tidal bar formation in cluster environments previously studied using controlled simulations and generalized the previous study (Łokas 2020), which considered only the most massive cluster of TNG100.

This work uses a higher-resolution simulation of the IllustrisTNG project, namely TNG50 (Nelson et al. 2019b; Pillepich et al. 2019), to study the properties of bar-like galaxies in the most massive cluster of this simulation box. The higher resolution allows the selection of objects with total stellar mass above $10^9\,\mathrm{M}_\odot$ (corresponding to around $10^4$ stellar particles), which remain suitable for morphological analysis. This choice enables the construction of a sample of 15 bar-like galaxies in a single cluster, whereas only a few such objects per cluster could be identified and followed in TNG100. The evolutionary paths of these galaxies can then be studied in the same environment, allowing a meaningful comparison between their histories.

The paper is organized as follows. Section 2 presents the main properties of the 15 selected bar-like galaxies and their evolution, focusing on the different measures of shape and the mass content. Section 3 describes the individual evolutionary paths of the galaxies, emphasizing their differences. Section 4 discusses the classification of the diverse evolutionary histories into groups with common features and demonstrates the coevolution of the bar-like galaxies and the forming cluster, in particular the build-up of its BCG through a series of mergers.

## 2. Formation and properties of the bar-like galaxies

This work uses the TNG50 simulation (Nelson et al. 2019b; Pillepich et al. 2019), the highest-resolution simulation of the IllustrisTNG project, performed in an approximately 50 Mpc box. The simulation includes baryonic particles with masses of $8.5 \times 10^4\,\mathrm{M}_\odot$ and dark matter particles with masses of $4.5 \times 10^5\,\mathrm{M}_\odot$, with corresponding softening scales of 0.074 and 0.288 kpc, respectively. The simulation data comprise 100 outputs, which provide sufficient time resolution to follow galaxy evolution. The data are publicly available, well documented, and easily retrievable, as described in Nelson et al. (2019a). The subhalos corresponding to galaxies are found using the Subfind algorithm (Springel et al. 2001), which assigns mass to them by locating locally overdense, self-bound particle groups within a larger parent group. Galaxies are identified by their subhalo ID numbers, which differ at subsequent outputs. Here, galaxies are referred to by their IDs in the last simulation output, corresponding to the present time ($t = 13.8\,\mathrm{Gyr}$, $z = 0$).

The most massive cluster of galaxies formed in this simulation has a BCG corresponding to the subhalo ID0. The total mass of this object at the end of the simulation is $2 \times 10^{14}\,\mathrm{M}_\odot$, which includes the stellar mass of $M_* = 5.4 \times 10^{12}\,\mathrm{M}_\odot$, the gas mass of $M_{\mathrm{gas}} = 2.3 \times 10^{13}\,\mathrm{M}_\odot$, and the dark mass of $M_{\mathrm{dm}} = 1.7 \times 10^{14}\,\mathrm{M}_\odot$. The BCG formed through major mergers of the cluster's most massive galaxies. This formation process significantly affected the evolution of other galaxies, including the bar-like galaxies discussed here.

The bar-like galaxies used in this study were selected among cluster members with a total stellar mass above $10^9\,\mathrm{M}_\odot$ at the final simulation output. This value corresponds to about $10^4$ stellar particles at TNG50 resolution, which enables morphological analysis. The TNG50 catalogs list 178 objects meeting this mass criterion, which reduces to 133 galaxies after removing dark-matter-free artifacts. To select bar-like galaxies, I applied a single criterion: the intermediate-to-longest axis ratio $b/a$ of the stellar component within two stellar half-mass radii, $2r_{1/2}$, had to be lower than 0.6. This condition was satisfied by 15 galaxies, whose IDs are listed in the first column of Table 1. The second column lists the values of their stellar half-mass radii, $r_{1/2}$. Figure 1 shows their images in terms of the surface density of the stars in the face-on view at the present time.

The axis ratio calculations followed the method of Genel et al. (2015) and agree with the values estimated by the Illustris team, provided in the Supplementary Data Catalogs of stellar circularities, angular momenta, and axis ratios. The eigenvalues of the stellar mass tensor provided the axis values after aligning each galaxy with its principal axes and calculating three components ($i = 1, 2, 3$): $M_i = (\Sigma_j m_j r_{j,i}^2 / \Sigma_j m_j)^{1/2}$, where $j$ enumerates over stellar particles, $r_{j,i}$ is the distance of stellar particle $j$ in the $i$-axis from the center of the galaxy, and $m_j$ is its mass. Sorting the eigenvalues so that $M_1 < M_2 < M_3$, yielded the shortest-to-longest axis ratio $c/a = M_1/M_3$ and the intermediate-to-longest axis ratio $b/a = M_2/M_3$. A useful combination of the axis ratios is the triaxiality parameter $T = [1 - (b/a)^2]/[1 - (c/a)^2]$, which measures the shape with

**Table 1.** Properties of the bar-like galaxies at $z = 0$.

| ID | $2r_{1/2}$ [kpc] | $M_*$ [$10^{10}$M$_\odot$] | $M_{\rm dm}$ [$10^{11}$M$_\odot$] | $b/a$ | $c/a$ | $T$ | $A_2$ | $f$ | $t_{\rm bf}$ [Gyr] | $A_{2,\rm max}$ | $R_{\rm bar}$ [kpc] | $d_{\rm ID0}$ [kpc] |
|---|---|---|---|---|---|---|---|---|---|---|---|---|
| 13 | 2.8 | 2.12 | 2.84 | 0.53 | 0.42 | 0.88 | 0.47 | 0.27 | 11.3 | 0.61 | 3.8 | 1793 |
| 14 | 4.7 | 2.76 | 1.51 | 0.59 | 0.41 | 0.79 | 0.45 | 0.28 | 8.1 | 0.58 | 4.9 | 1291 |
| 15 | 2.7 | 3.33 | 0.81 | 0.57 | 0.40 | 0.81 | 0.30 | 0.23 | 10.2 | 0.65 | 4.4 | 701 |
| 23 | 2.0 | 1.82 | 1.09 | 0.56 | 0.48 | 0.90 | 0.37 | 0.10 | 5.9 | 0.55 | 2.3 | 428 |
| 31 | 2.2 | 1.49 | 0.44 | 0.56 | 0.48 | 0.88 | 0.40 | 0.10 | 7.6 | 0.60 | 2.1 | 443 |
| 34 | 3.2 | 1.25 | 0.55 | 0.56 | 0.43 | 0.84 | 0.38 | 0.12 | 6.5 | 0.53 | 6.0 | 720 |
| 35 | 3.2 | 1.43 | 0.34 | 0.49 | 0.41 | 0.91 | 0.48 | 0.10 | 3.6 | 0.64 | 4.1 | 503 |
| 38 | 3.0 | 1.39 | 0.19 | 0.60 | 0.46 | 0.82 | 0.43 | 0.12 | 5.0 | 0.55 | 3.5 | 488 |
| 42 | 1.6 | 1.39 | 0.07 | 0.55 | 0.47 | 0.89 | 0.38 | 0.07 | 3.1 | 0.58 | 2.1 | 133 |
| 55 | 3.5 | 0.87 | 0.21 | 0.53 | 0.43 | 0.89 | 0.49 | 0.05 | 8.6 | 0.59 | 5.1 | 158 |
| 64 | 3.1 | 0.67 | 0.20 | 0.55 | 0.47 | 0.89 | 0.44 | 0.08 | 9.2 | 0.55 | 4.2 | 313 |
| 71 | 2.7 | 0.67 | 0.09 | 0.53 | 0.41 | 0.87 | 0.46 | 0.06 | 9.7 | 0.57 | 4.5 | 261 |
| 72 | 2.1 | 0.68 | 0.07 | 0.56 | 0.46 | 0.87 | 0.41 | 0.04 | 8.4 | 0.55 | 2.9 | 114 |
| 87 | 3.1 | 0.52 | 0.08 | 0.56 | 0.45 | 0.86 | 0.39 | 0.04 | 6.7 | 0.51 | 5.1 | 148 |
| 308 | 0.9 | 0.10 | 0.003 | 0.50 | 0.50 | 0.99 | 0.44 | 0.06 | 3.1 | 0.62 | 3.3 | 596 |
| Median | 2.8 | 1.39 | 0.21 | 0.56 | 0.45 | 0.88 | 0.43 | 0.10 | 7.6 | 0.58 | 4.1 | 443 |

a single value. Values of $T < 1/3$ correspond to strongly oblate objects, $T > 2/3$ to strongly prolate objects, and intermediate values correspond to triaxial shapes.

In addition to shape measures, it is useful to consider the kinematics of the stellar component, particularly the amount of rotational support in the galaxy. This was measured for TNG50 galaxies using the rotation parameter, $f$, defined as the fractional mass of all stars with the circularity parameter $\epsilon > 0.7$, where $\epsilon = J_z/J(E)$, $J_z$ is the specific angular momentum of the star along the angular momentum of the galaxy, and $J(E)$ is the maximum angular momentum of stellar particles (Genel et al. 2015). This parameter reliably measures the amount of rotation in the galaxy, with $f > 0.4$ considered characteristic of disks (Joshi et al. 2020). Figure 2 shows the measures of shape and kinematics as a function of time for all 15 bar-like galaxies, and the parameter values at the end of the evolution are listed in Table 1 (columns 5–7, 9).

The evolution of the bar is best quantified using the commonly adopted measure of bar strength (Athanassoula & Misiriotis 2002), namely the $m = 2$ Fourier mode of surface density projected along the short axis. This is given by $A_2(R) = |\Sigma_j m_j \exp(2i\theta_j)|/\Sigma_j m_j$, where $\theta_j$ is the azimuthal angle of the $j$th star, $m_j$ is its mass, and the sum goes up to the number of particles in a given radial bin. Figure 2 shows the measurements of the bar mode using stars within two stellar half-mass radii, $2r_{1/2}$ (black line). The bar formation time $t_{\rm bf}$ corresponds to the moment when $A_2(<2r_{1/2})$ crosses 0.2 and remains above this value until the end of the evolution; a vertical dashed line marks it in each case. Table 1 lists the values of $A_2(<2r_{1/2})$ at the end of the evolution and the bar formation times in the eighth and tenth columns, respectively.

The axis ratio $b/a$ and the bar mode $A_2$ provide alternative measures of shape: $A_2$ uses a projected distribution of stars, whereas $b/a$ takes into account the 3D shape (because it implicitly assumes $c < b$). The criterion $b/a < 0.6$ is convenient initially, as $b/a$ values are provided in the TNG50 data release. While $b/a$ and $A_2$ remain strongly correlated at all times, with $A_2 = 0.2$ corresponding roughly to $b/a = 0.8$, the $A_2$ threshold is preferable to characterize the bars at early times because it appears more stable.

The evolution of shape and kinematic measures in Fig. 2 exhibits common features across all galaxies. Although the bar formation times differ, bar formation always produces a strongly increasing value of triaxiality $T$ and a decreasing value of $b/a$, while rotation decreases due to the more radial orbits of stars within the bar. Additionally, the evolution of the rotation parameter $f$ often shows sudden drops, which sometimes coincide with bar formation. These decreases in rotation typically result from tidal forces acting on the galaxy during interactions with a massive companion. These interactions also produce sudden drops in the galaxy's bound mass.

To verify this, Fig. 3 shows the evolution of each galaxy's total mass in three components: dark matter, stars, and gas. All galaxies grew in mass until experiencing a sudden drop, particularly in the dark component and the gas, while the stellar mass was much less affected. Stellar masses reached a maximum and ceased growing due to the lack of gas, then declined slowly. The sudden drops in dark mass content coincide with the drops in the rotation parameters shown in Fig. 2. The total stellar and dark masses of the galaxies at the end of the evolution are listed in the third and fourth columns of Table 1. The galaxies lost their gas by that time, except for ID13 and ID15, which retained a small gas mass of $10^7$ M$_\odot$.

To identify the sources of the tidal force, I searched the simulation data for neighbors of the 15 galaxies at times when their shape and mass content evolved most strongly. This allowed me to identify perturbers that were massive and close enough to affect the galaxies under study. Figure 4 shows the relative distances between each galaxy and the perturbers most likely to influence its evolution. The minima of the distances correspond to the pericenter passages, where the interactions are strongest. In all panels, the blue line shows the distance to the most massive progenitor of the BCG (ID0) and the figure demonstrates that each galaxy experienced at least one pericenter passage around it. The present-day distances of the galaxies from ID0 are listed in the last column of Table 1. However, this interaction was not the most important one for some galaxies and, in a few cases, other galaxies and mergers played an important role. Details of these interactions are described in the next section.

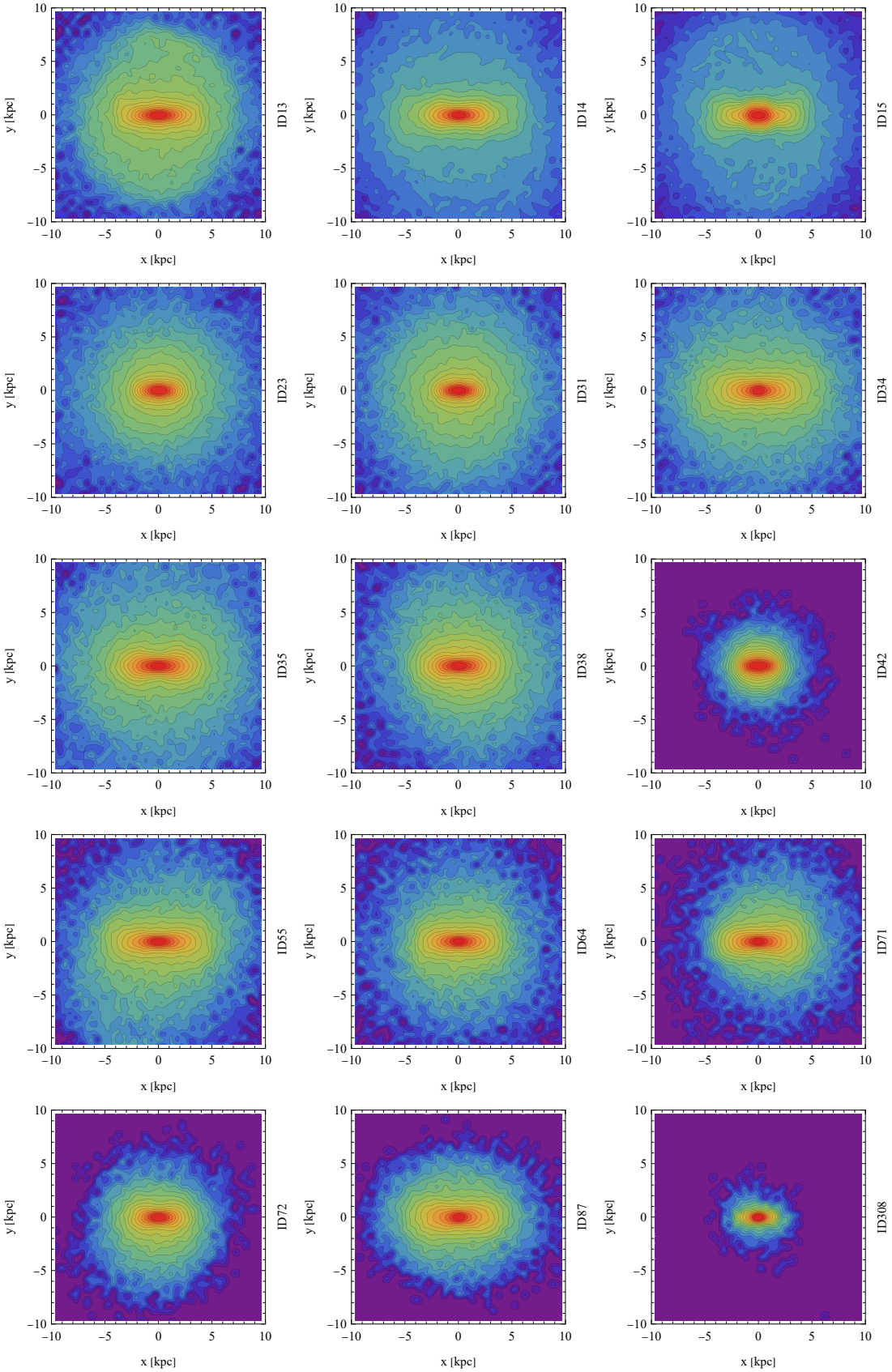


**Fig. 1.** Surface density maps of the stellar component of 15 bar-like galaxies in face-on view at $z = 0$. Galaxies are identified by their subhalo ID numbers at $z = 0$, shown on the right of each panel. The color scale is adjusted to the maximum and minimum density of each galaxy and the contours are equally spaced in log surface density.

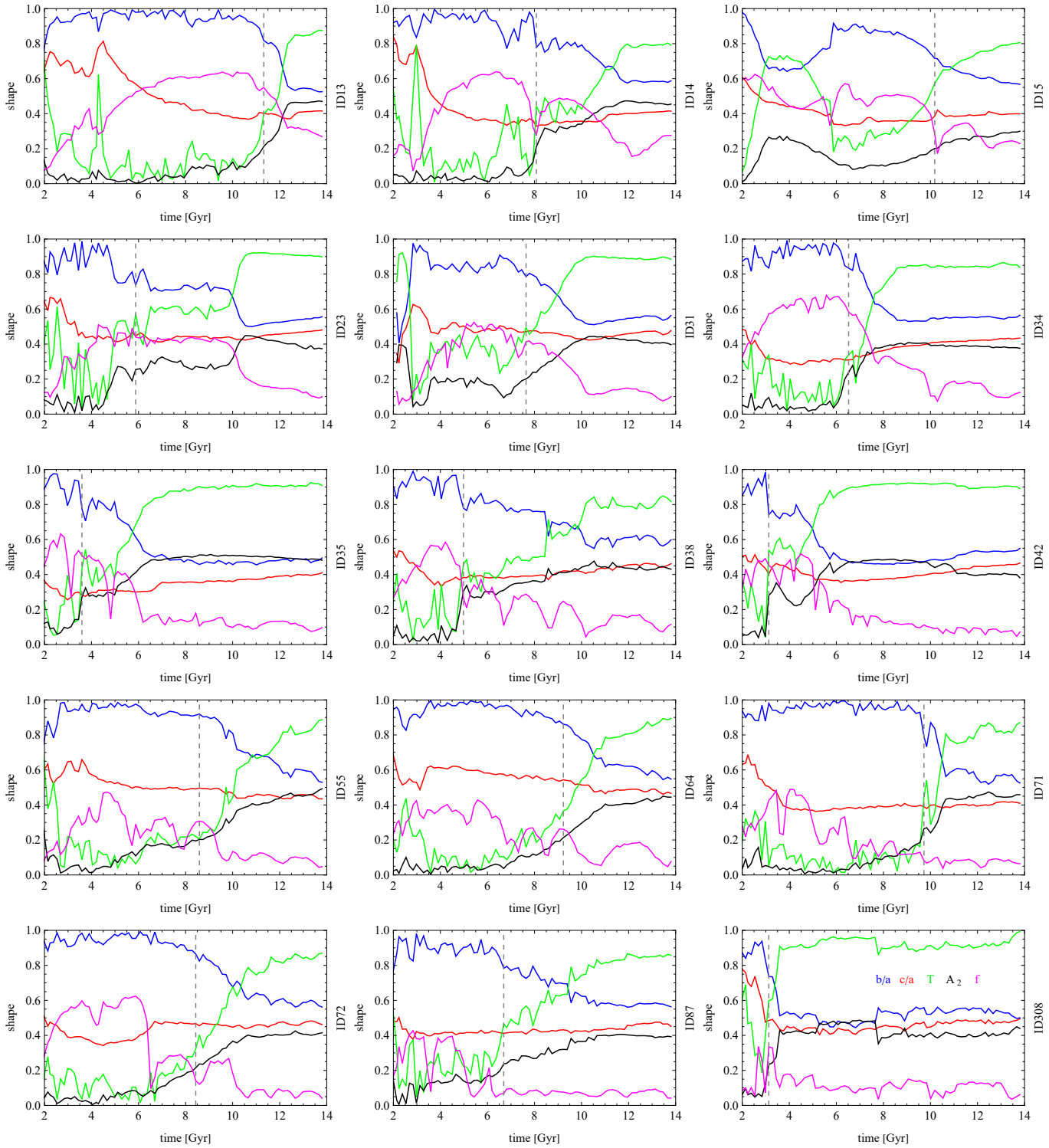


**Fig. 2.** Evolution of different measures of shape over time for 15 bar-like galaxies. Lines show the axis ratios $b/a$ (blue), $c/a$ (red), the triaxiality parameter $T$ (green), the rotation parameter $f$ (magenta), and the bar mode $A_2$ (black). Galaxies are identified by their subhalo ID numbers at $z = 0$, shown on the right of each panel. Vertical dashed lines indicate the time of bar formation.

Finally, Figs. 5–7 illustrate the detailed evolution of galaxy shapes through the bar mode profiles as a function of time, $A_2(R, t)$. The bar mode was measured in bins of $\Delta R = 0.5$ kpc out to 15 kpc in cylindrical radius. The color-coded maps show a persistent bar-like shape near the galaxy center and the elongations of each galaxy at larger radii caused by interactions. Redder colors indicate stronger elongations, which reach their extremes at the outskirts where tidal tails appear. These outer regions become increasingly sparsely populated, and the reddest shade corresponds to regions where no stars are bound to the galaxy due to tidal stripping. These measurements can also be used to estimate the bar length. The typical shape of the $A_2(R)$

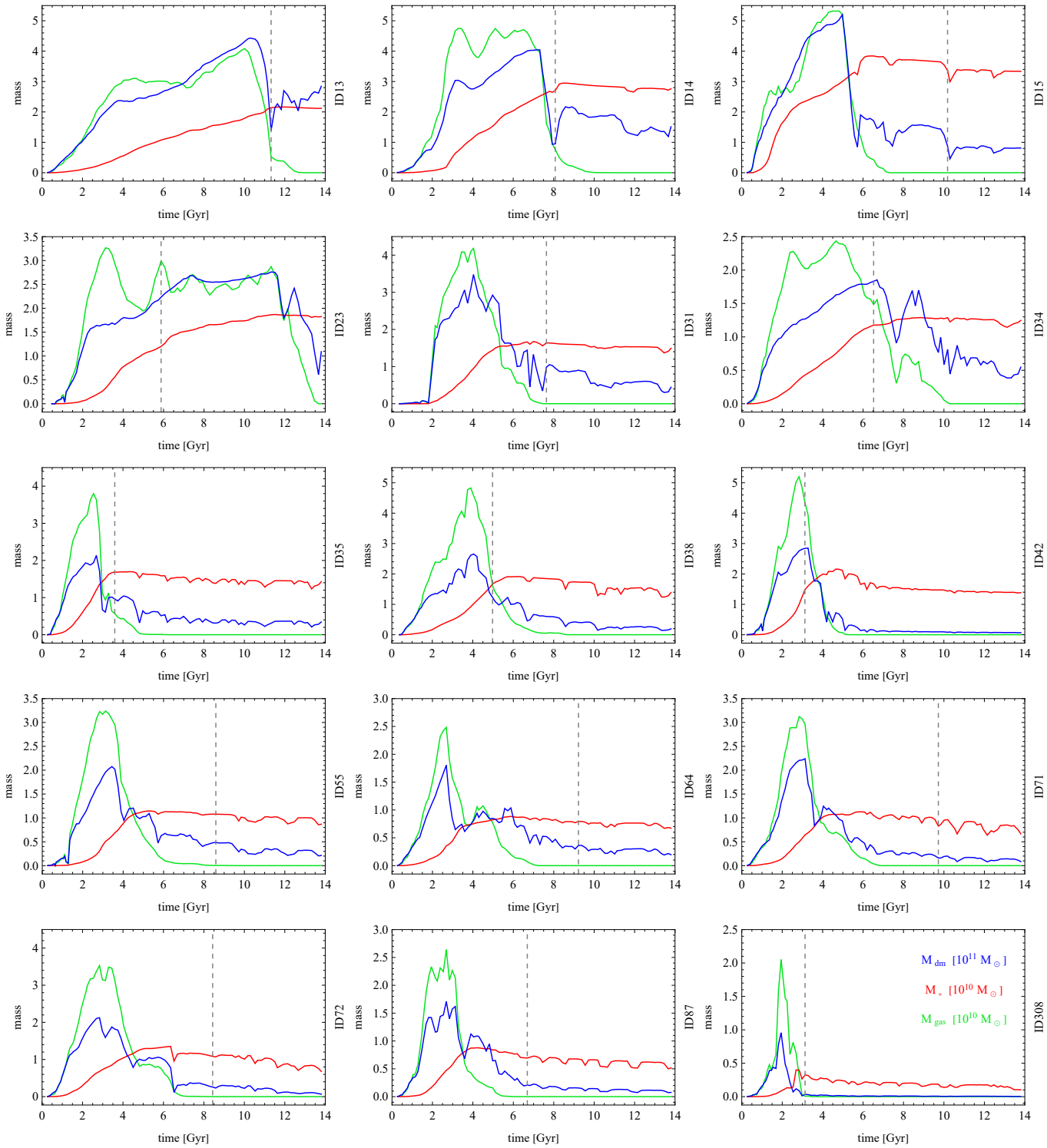


**Fig. 3.** Evolution of the total mass over time for 15 bar-like galaxies. Lines show the total galaxy mass in dark matter (blue), stars (red), and gas (green). The dark masses are given in units of $10^{11}$ $M_\odot$, while the stellar and gas masses are in units of $10^{10}$ $M_\odot$. Galaxies are identified by their subhalo ID numbers at $z = 0$, shown on the right of each panel. Vertical dashed lines indicate the time of bar formation.

profile for a barred galaxy rises to a maximum value, $A_{2,\max}$, and then decreases, except during temporary strong tidal distortions, when a secondary rise occurs at larger radii. The bar length can be estimated as the radius $R_{\rm bar}$ where $A_2(R)$ drops to $A_{2,\max}/2$. Table 1 lists the values of $A_{2,\max}$ and $R_{\rm bar}$ at the end of the evolution in the 11th and 12th columns.

## 3. Individual evolutionary tracks

This section presents the different evolutionary histories of the galaxies inferred from the results presented in Figs. 1–7. The galaxies are described in the same order, in which they are listed in Table 1.

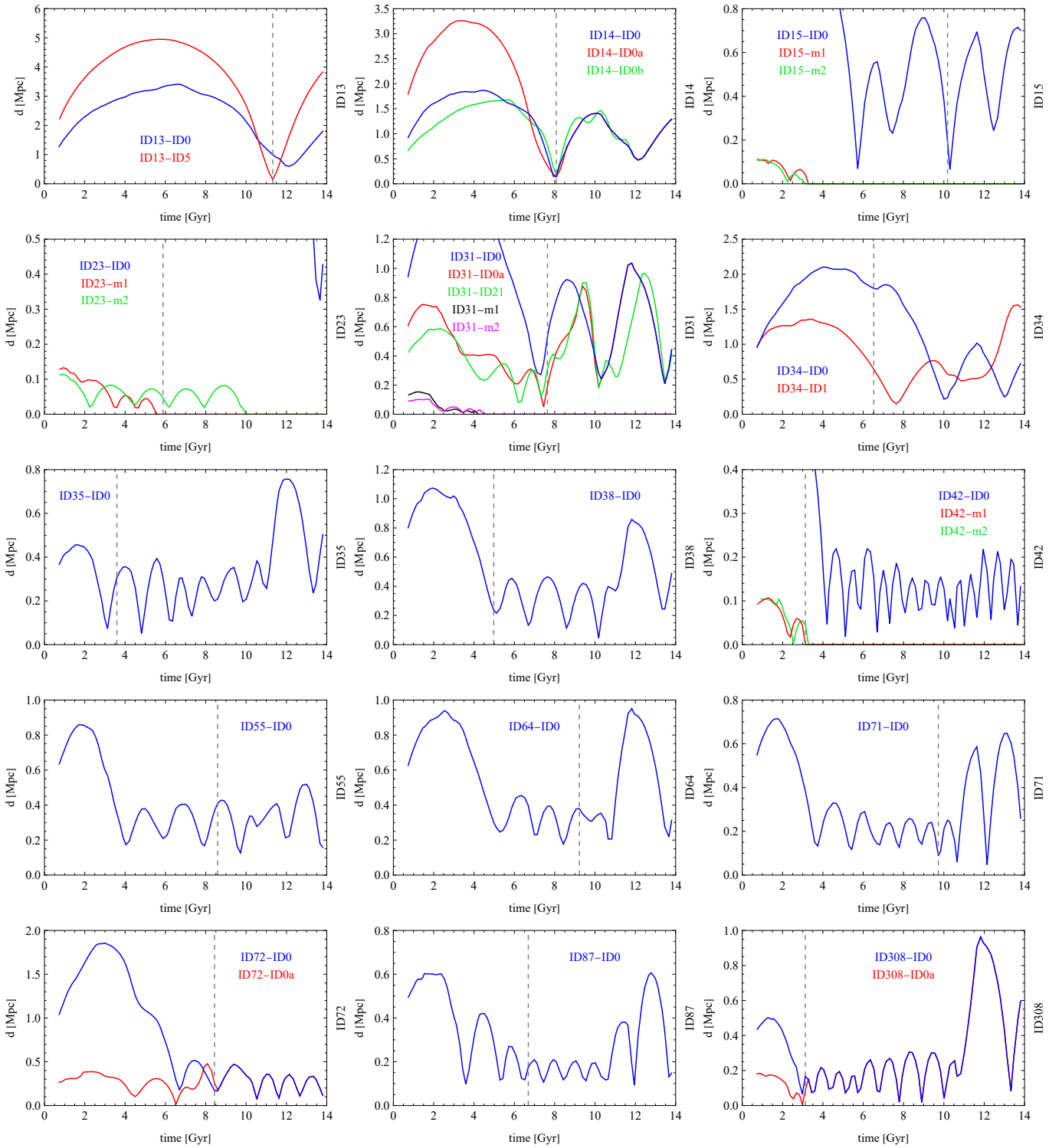


**Fig. 4.** Distances from perturbers as a function of time for 15 bar-like galaxies. Different colored lines show the distances from distinct perturbers, with data for ID0 shown in blue in all panels. Galaxies are identified by their subhalo ID numbers at $z = 0$, shown on the right of each panel. Vertical dashed lines indicate the time of bar formation.

ID13 The galaxy was a late and short-time visitor to the cluster and is now at its outskirts. It approached ID0 and its companions around 11 Gyr and its bar formed at 11.3 Gyr during the interaction with ID5 at a pericenter distance of $r_{\rm peri} = 150$ kpc; ID5 had a mass of $3.6 \times 10^{11}$ $M_\odot$ at that time. The tidal force was not particularly strong, but it was likely sufficient to strengthen the small bar-like perturbation already present at 8.5 Gyr. The bar was further enhanced at 12.1 Gyr when the galaxy interacted with ID0 (with $r_{\rm peri} = 602$ kpc), which had a mass of $2 \times 10^{14}$ $M_\odot$ at that time.

ID14 The bar was induced at 8.1 Gyr after a strong interaction ($r_{\rm peri} = 151$ kpc) with the most massive progenitor of ID0, which had a mass of $8.6 \times 10^{13}$ $M_\odot$ at that time. Simultaneously, the

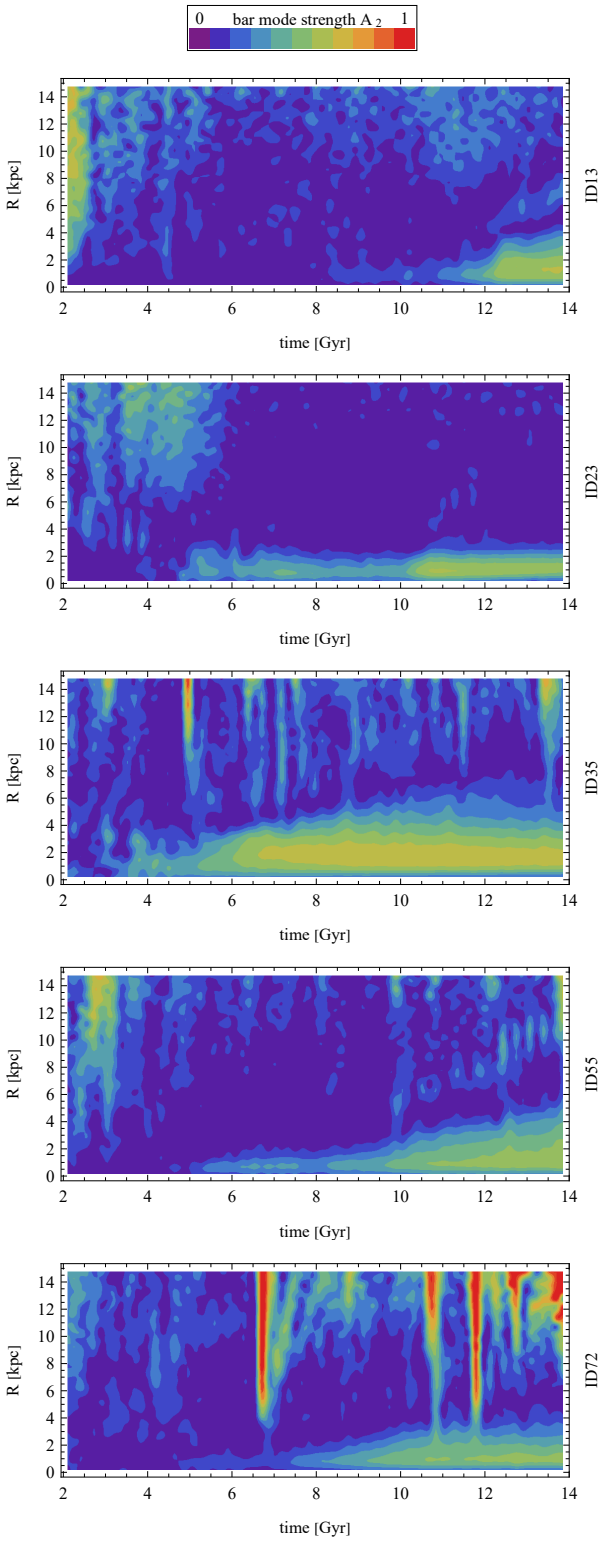


**Fig. 5.** Evolution of the profile of the bar mode, $A_2(R)$, over time for five galaxies from the first columns of Figs. 1–4. The galaxies are identified by their subhalo ID numbers at $z = 0$ given on the right of each panel. The reddest color corresponds to regions with no stars bound to the galaxy.

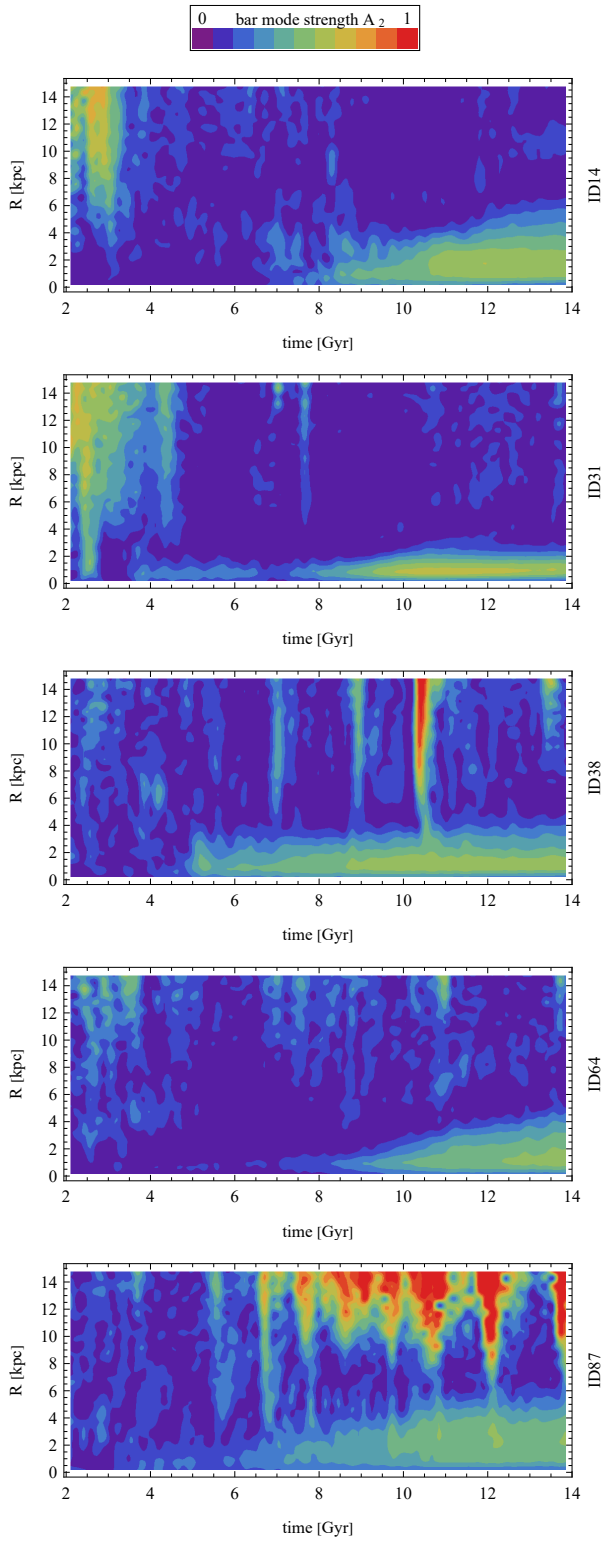


**Fig. 6.** Same as Fig. 5, but for five galaxies from the second columns of Figs. 1–4.

galaxy interacted with two smaller progenitors of ID0 (ID0a and ID0b in Fig. 4), which later merged with the BCG. The masses of these progenitors were both below $10^{12}\,M_\odot$, while their pericenters were comparable to the one of the main perturber.

ID15 This galaxy formed a small bar as early as 3 Gyr, likely due to minor mergers (m1 and m2 in Fig. 4, both with masses above $10^9\,M_\odot$ before the interactions) and flybys of small satellites. The first pericenter passage around ID0 (with $r_{\rm peri}$ = 69 kpc) at 6 Gyr destroyed the bar. A third pericenter around the same perturber at 10 Gyr (with $r_{\rm peri}$ = 66 kpc) strengthened

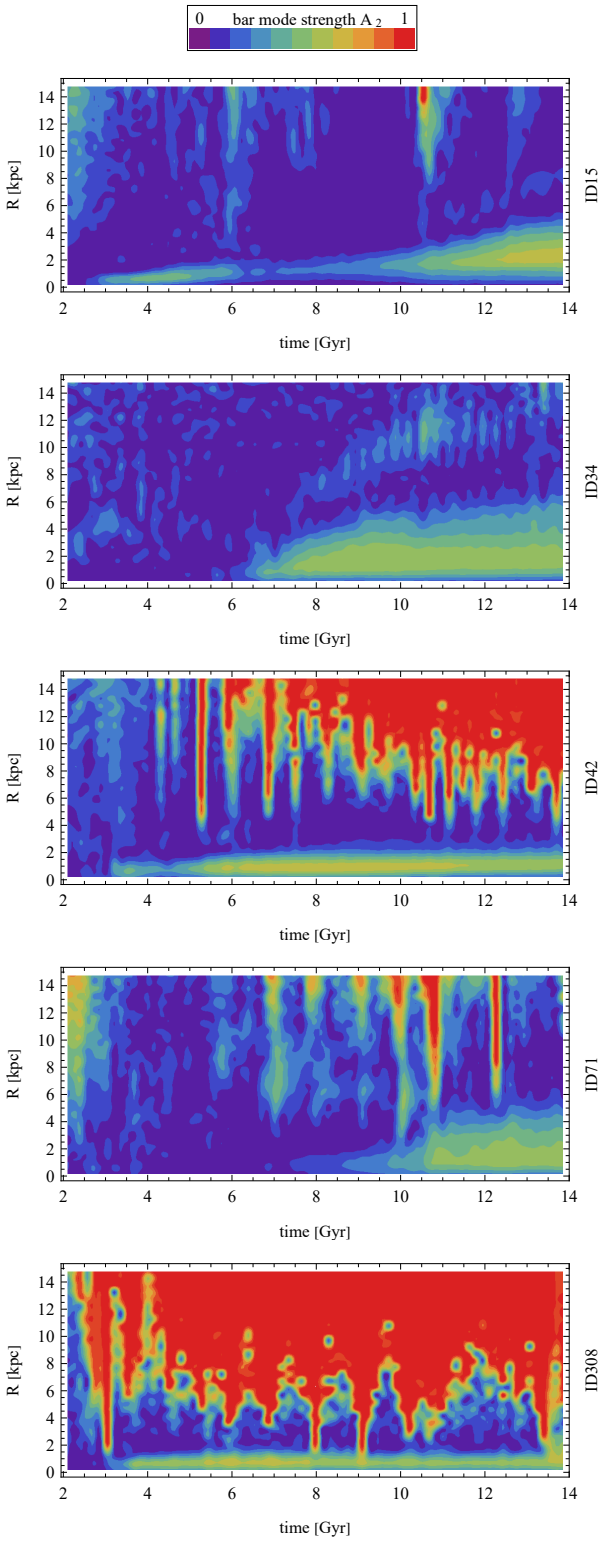


**Fig. 7.** Same as Fig. 5, but for five galaxies from the third columns of Figs. 1–4.

the bar again, allowing it to survive until today. The satellites of ID15 that may have contributed to the initial bar formation later merged with ID0 during and after the first pericenter.

ID23 The bar in this galaxy began to form around 5 Gyr and was strongly enhanced at 10 Gyr, likely due to mergers with small satellites (m1 and m2 in Fig. 4). The galaxy only recently entered the cluster and experienced one pericenter passage around ID0 ($r_{\rm peri}$ = 325 kpc), which was sufficient to remove all its gas and most of its dark matter but left the bar unaffected.

ID31 This galaxy formed a small bar as early as 3.5 Gyr, likely as a result of interactions and mergers with smaller satellites. An interaction with the more massive galaxy ID21 at 6.5 Gyr weakened the bar. The permanent bar formed shortly afterward, at 7.6 Gyr, following interactions with two massive progenitors of ID0.

ID34 Inherent disk instability or very small mergers triggered the formation of the bar in this galaxy at 6.5 Gyr. Interaction with the very massive galaxy ID1 at 7.6 Gyr increased the bar's strength. The galaxy entered the cluster much later and experienced two pericenter passages around ID0, at 10 and 13 Gyr, which had little effect on the bar.

ID35 The bar formed at 3.6 Gyr after the first pericenter (with $r_{\rm peri}$ = 74 kpc) around the most massive progenitor of ID0 and was enhanced at the second pericenter. The bar remained stable in its strength and length afterward as the galaxy's orbit became more extended. This case represents a classical example of a bar tidally induced by interaction with a cluster BCG.

ID38 The galaxy formed a bar at 5 Gyr during the first pericenter passage (with $r_{\rm peri}$ = 216 kpc) around the most massive progenitor of ID0 and remained on a tight orbit until this progenitor merged with another massive galaxy, which changed the orbital configuration. The bar strengthened during the third pericenter passage at 8.6 Gyr, while the tightest pericenter around 10 Gyr had little effect. This case represents a relatively simple example of bar formation in the cluster environment.

ID42 The bar was formed very early, at 3.1 Gyr, likely due to the last minor mergers the galaxy experienced. The bar weakened slightly after the first pericenter passage around a progenitor of ID0 and strengthened again after the second pericenter. The galaxy remained on a very tight orbit around ID0 until the end of the evolution and was heavily stripped of mass. The bar remained short enough to avoid strong effects from close encounters, except for minor weakening around 11 Gyr after several particularly tight pericenter passages.

ID55 The galaxy started to form a bar around 6 Gyr after the second pericenter passage around a progenitor of ID0. The bar reached the bar formation threshold at 8.6 Gyr, after the third pericenter, and strengthened further following the fourth pericenter passage at 10 Gyr. It continued to grow steadily until the present.

ID64 The bar formed at 9.2 Gyr after the third pericenter passage around the most massive progenitor of ID0 and grew steadily before and after that time, with the length slightly increasing after the next pericenter passage at around 11 Gyr. During the formation period, the galaxy also interacted with a few other progenitors of ID0, which makes the case less clear.

ID71 Bar growth began at 7.5 Gyr following the third pericenter passage around ID0. The bar fully formed at the sixth pericenter at 9.7 Gyr and strengthened further at the next, very tight pericenter at 10.7 Gyr. Another tight pericenter at 12.1 Gyr did not strongly affect its properties.

ID72 A small elongation was already present in this galaxy at 5 Gyr, which grew after a strong interaction with the two most massive progenitors of ID0 around 6.5-6.7 Gyr. The less massive progenitor (ID0a) exerted a stronger tidal force because the pericenter distance in this case was much smaller ($r_{\rm peri} = 18$ kpc). The bar grew steadily and fully formed at 8.4 Gyr during the second pericenter around the more massive progenitor of ID0. Interestingly, this is also when the two progenitors of ID0 merge. Further strong interactions with the merged ID0 did not significantly affect the bar.

ID87 The bar began to form around 4 Gyr after the first pericenter passage around one of the massive progenitors of ID0 and fully formed at 6.7 Gyr after the third pericenter. The galaxy remained on a tight orbit around ID0 and was heavily stripped, while subsequent pericenter passages made the bar longer and stronger.

ID308 This is the smallest and most heavily stripped galaxy in the sample, although its dark matter mass reached almost $10^{11}\,{\rm M}_\odot$ before interactions. The bar formed very early, at 3.1 Gyr, through interactions with a massive progenitor of ID0 and a less massive one (ID0a), which soon merged with the more massive progenitor. The tidal force of the less massive progenitor, with a mass of $5 \times 10^{11}\,{\rm M}_\odot$ at 3 Gyr was greater because it passed ID308 at a very small $r_{\rm peri} = 6$ kpc, whereas the more massive progenitor, with a mass $1.5 \times 10^{13}\,{\rm M}_\odot$ had $r_{\rm peri} = 65$ kpc. The galaxy remained on a very tight orbit around ID0 and the subsequent pericenter passages slightly strengthened the bar around 5 Gyr and weakened it at 8 Gyr, but it survived until the present.

## 4. Discussion

This study examined the properties of bar-like galaxies in the most massive cluster of TNG50. The last row of Table 1 lists the median values of their main parameters at the end of the evolution. In addition to their defining feature, a strongly prolate stellar component, the only properties these galaxies share are strong mass loss and the lack of gas and star formation. Although clusters generally contain galaxies with these features, the bar-like sample appears to be rather extreme in this respect. In particular, only two out of 15 galaxies (13%) in the sample have some (very low) gas content of around $10^7\,{\rm M}_\odot$, whereas 29% of all 133 galaxies in the cluster have nonzero gas content, and 14% have significant gas mass above $10^9\,{\rm M}_\odot$. None of the 15 bar-like galaxies form stars at $z = 0$, whereas 17% of the total sample still have nonzero star formation rates. All 15 bar-like galaxies are red with $g - r > 0.74$ mag, while 86% of the total sample are red with $g - r > 0.6$, and only 60% are as red as the bar-like galaxies ($g - r > 0.74$). All the bar-like galaxies are thus red and dead and would be classified as typical ellipticals unless viewed exactly face-on, in which case their shapes would appear more elongated.

The low gas content and early quenching may have facilitated bar formation. Most of the bars studied here form when the galaxy is completely stripped of gas, which strongly suggests that the bars form more easily when the gas fraction is low. Figure 3 shows that, for 11 of the 15 galaxies, there is no gas left when the bar forms or its mass is much smaller than the mass of stars. In cases when the total gas mass equals or exceeds the stellar mass at that time (IDs: 23, 34, 38, and 42), the gas mass within $2r_{1/2}$ (where the bar forms) remains much lower than the stellar mass.

All 15 galaxies (except ID13) lost more than half, and often much more, of their maximum dark mass. These mass loss features are expected because the galaxies were selected as cluster members and therefore must have interacted with the BCG or other galaxies during their evolution. All galaxies experienced at least one, and often multiple, pericenter passages around the BCG (ID0), so none are infalling into the cluster for the first time.

However, the similarities between galaxies end here. Beyond these definition-related properties, the galaxies follow very different evolutionary histories. Some galaxies experienced strong interactions with the BCG and were heavily stripped, even in the stellar component, as shown in Figs. 1, 3, and 5–7. This subsample includes ID42, ID71, ID72, ID87, and ID308. Among these, ID308 experienced particularly strong stripping and is the smallest and least massive galaxy in the sample. In this respect, it is similar to the Sagittarius-like object studied in Łokas (2024), except that it evolved around a BCG rather than a Milky Way-like galaxy. The remaining galaxies of the sample evolved on less tight orbits. The ID13 and ID23 galaxies exemplify the other extreme: the least affected galaxies, each with only a single pericenter passage around ID0 in their history. The galaxies span a wide range of distances from the cluster center, from 114 kpc (ID72) to 1.8 Mpc (ID13). Strongly stripped galaxies typically lie closer (the last column of Table 1), though this is not always the case, as discussed below.

The galaxies also exhibit strong differences in bar formation times, bar properties, and formation mechanisms. The bar formation times (tenth column of Table 1) range from 3.1 to 11.3 Gyr, with the median value of 7.6 Gyr. In the cases of bars induced by interactions, the bars form between 0–0.8 Gyr after pericenter passage, with an uncertainty of 0.1–0.2 Gyr following from the time difference between the available simulation outputs. The ID42 and ID308 galaxies both formed their bars at the earliest time of 3.1 Gyr, but through different mechanisms: minor mergers in ID42 and interaction with a progenitor of ID0 in ID308. These formation times are later, and the bar lengths are shorter than those of the best candidates for the analogs of high-redshift bars discovered with JWST selected from TNG100 in Łokas (2025a,c).

All bars are strong at the final time, with $A_{2,\rm max} > 0.5$ and a median of 0.58, reflecting the selection criterion of a strongly prolate shape, $b/a < 0.6$. However, the bars have very different lengths, from 2.1 to 6 kpc (median 4.1 kpc), and show little correlation between the bar length and orbit tightness or the amount of stripping the galaxy experienced. This is because interactions can shorten bars through tidal stripping or lengthen them when tidally induced. The bar of ID308 provides a good example of the latter case, as it remained short for most of its history and only elongated after the last pericenter passage. The bar pattern speeds also vary significantly and range between $9{-}27\,{\rm km\,s^{-1}\,kpc^{-1}}$. These values were estimated at $z = 0$ using the Tremaine & Weinberg (1984) method for the first eight galaxies in Table 1. The remaining objects are strongly perturbed by recent interactions and their pattern speeds cannot be reliably measured.

Overall, interaction with one of the progenitors of ID0 tidally induced or strongly enhanced the bars in 11 of the 15 galaxies, but only ID35 formed its bar directly after the first pericenter passage around a single most massive progenitor of ID0. In two cases (ID23 and ID42) the formation of the bar could be related to mergers with smaller satellites, while a passage near another massive galaxy likely drove bar formation in ID13. In ID34, inherent disk instability likely formed the bar, although the role of minor mergers cannot be completely excluded. In ID15, the bar formed early by mergers was destroyed at the first pericenter passage around ID0 and formed again at the third pericenter.

Despite the different origins, the subsequent evolution of the bars was to some extent affected by the following pericenter passages around the BCG. The only exception to this rule is ID23, which had only one very recent and distant passage and is the only galaxy in the sample that can be described as having evolved in isolation, as evidenced by no tidal features at large radii visible in Fig. 5. However, even for galaxies that interacted strongly with the progenitors of ID0, the impact of these interactions varied significantly between objects and even subsequent pericenters for the same galaxy. This is probably due to the orientation of the bar at the pericenter, which results from a random combination of the bar pattern speed and the galaxy's velocity on the orbit. As described in detail in Łokas et al. (2014), the tidal force from the perturber can weaken or strengthen the bar depending on this orientation.

The resolution of the TNG50 simulation may influence the results of this study. The selection required galaxies to have a stellar mass above $10^9\,M_\odot$ at the end of evolution, corresponding to about $10^4$ stellar particles, to enable morphological analysis. Observations of cluster galaxy populations (Méndez-Abreu et al. 2023) indicate that barred galaxies rarely occur below this stellar mass. This suggests that the sample considered here is representative of the bar-like population in clusters. Frankel et al. (2022) demonstrated that the resolution mostly affects the bar pattern speeds (which are underestimated in low-resolution simulations), rather than other properties such as the bar length. Since the pattern speeds are difficult to measure for the bar-like objects studied in this work (as stated above), this issue should not be of concern here. Other bar properties, particularly their evolutionary histories, which are the focus of this work, should not be very sensitive to resolution.

In summary, this analysis reveals that the formation and evolution of bar-like galaxies in the cluster environment differ strongly from the idealized scenario of controlled simulations, such as presented in Łokas et al. (2016), where a Milky Way-like galaxy was placed on an orbit around a preexisting cluster. The bar-like galaxies in this study witnessed the formation of the BCG and coevolved with its progenitors. Most bar formation events and subsequent interactions occurred before the BCG was fully formed. The bar-like galaxies interacted with multiple progenitors of ID0, including two (ID31, ID72,and ID308) or three at once (ID14). In three cases (ID14, ID72, and ID308), these interactions and bar formation occurred immediately before the progenitors of ID0 merged. For six bar-like galaxies, the merger events leading to the final formation of the BCG later on (around 11 Gyr) led to significant alterations of their orbits around the BCG. These galaxies were ejected on more extended orbits which led to fewer (if not less tight) pericenter passages. This may explain why some of the bar-like galaxies (in particular ID308) survived until the present.

The significance of this complicated scenario and its implications for the efficiency of bar formation in clusters deserve further study. It remains unclear what would happen if the configuration were simpler, that is, if the BCG formed earlier and the other galaxies interacted with a single object rather than several of its massive progenitors. Studying clusters with BCGs that have different formation histories could address this question, although drawing firm conclusions may remain challenging due to random variations in cluster properties such as mass and composition.

*Acknowledgements.* I am grateful to the IllustrisTNG team for making their simulations publicly available and to the anonymous reviewer for useful comments. This work was supported in part by the National Science Centre of Poland with grant 2025/57/B/ST9/00321. Computations for this work were performed using the computer cluster at the Nicolaus Copernicus Astronomical Center of the Polish Academy of Sciences (CAMK PAN).

## References

Aguerri, J. A. L., Cuomo, V., Rojas-Roncero, A., & Morelli, L. 2023, A&A, 679, A5
Amvrosiadis, A., Lange, S., Nightingale, J. W., et al. 2025, MNRAS, 537, 1163
Andersen, V. 1996, AJ, 111, 1805
Athanassoula, E. 2003, MNRAS, 341, 1179
Athanassoula, E., & Misiriotis, A. 2002, MNRAS, 330, 35
Barazza, F. D., Jablonka, P., Desai, V., et al. 2009, A&A, 497, 713
Berentzen, I., Athanassoula, E., Heller, C. H., & Fricke, K. J. 2004, MNRAS, 347, 220
Cervantes Sodi, B., Li, C., & Park, C. 2015, ApJ, 807, 111
Costantin, L., Pérez-González, P. G., Guo, Y., et al. 2023, Nature, 623, 499
Frankel, N., Pillepich, A., Rix, H.-W., et al. 2022, ApJ, 940, 61
Gajda, G., Łokas, E. L., & Athanassoula, E. 2017, ApJ, 842, 56
Gajda, G., Łokas, E. L., & Athanassoula, E. 2018, ApJ, 868, 100
Genel, S., Fall, S. M., Hernquist, L., et al. 2015, ApJ, 804, L40
Gerin, M., Combes, F., & Athanassoula, E. 1990, A&A, 230, 37
Géron, T., Smethurst, R. J., Dickinson, H., et al. 2025, ApJ, 987, 74
Guo, Y., Jogee, S., Finkelstein, S. L., et al. 2023, ApJ, 945, L10
Guo, Y., Jogee, S., Wise, E., et al. 2025, ApJ, 985, 181
Hohl, F. 1971, ApJ, 168, 343
Joshi, G. D., Pillepich, A., Nelson, D., et al. 2020, MNRAS, 496, 2673
Lansbury, G. B., Lucey, J. R., & Smith, R. J. 2014, MNRAS, 439, 1749
Le Conte, Z. A., Gadotti, D. A., Ferreira, L., et al. 2024, MNRAS, 530, 1984
Łokas, E. L. 2018, ApJ, 857, 6
Łokas, E. L. 2020, A&A, 638, A133
Łokas, E. L. 2021, A&A, 647, A143
Łokas, E. L. 2024, A&A, 687, A82
Łokas, E. L. 2025a, A&A, 700, A258
Łokas, E. L. 2025b, A&A, 702, A7
Łokas, E. L. 2025c, ApJ, 991, L52
Łokas, E. L., Athanassoula, E., Debattista, V. P., et al. 2014, MNRAS, 445, 1339
Łokas, E. L., Semczuk, M., Gajda, G., & D'Onghia, E. 2015, ApJ, 810, 100
Łokas, E. L., Ebrová, I., del Pino, A., et al. 2016, ApJ, 826, 227
Marinacci, F., Vogelsberger, M., Pakmor, R., et al. 2018, MNRAS, 480, 5113
Mastropietro, C., Moore, B., Mayer, L., et al. 2005, MNRAS, 364, 607
Méndez-Abreu, J., Sánchez-Janssen, R., & Aguerri, J. A. L. 2010, ApJ, 711, L61
Méndez-Abreu, J., Costantin, L., & Kruk, S. 2023, A&A, 678, A5
Miwa, T., & Noguchi, M. 1998, ApJ, 499, 149
Naiman, J. P., Pillepich, A., Springel, V., et al. 2018, MNRAS, 477, 1206
Nelson, D., Pillepich, A., Springel, V., et al. 2018, MNRAS, 475, 624
Nelson, D., Springel, V., Pillepich, A., et al. 2019a, Comput. Astrophys. Cosmol., 6, 2
Nelson, D., Pillepich, A., Springel, V., et al. 2019b, MNRAS, 490, 3234
Noguchi, M. 1987, MNRAS, 228, 635
Ostriker, J. P., & Peebles, P. J. E. 1973, ApJ, 186, 467
Peschken, N., & Łokas, E. L. 2019, MNRAS, 483, 2721
Pillepich, A., Nelson, D., Hernquist, L., et al. 2018, MNRAS, 475, 648
Pillepich, A., Nelson, D., Springel, V., et al. 2019, MNRAS, 490, 3196
Rosas-Guevara, Y., Bonoli, S., Dotti, M., et al. 2020, MNRAS, 491, 2547
Rosas-Guevara, Y., Bonoli, S., Dotti, M., et al. 2022, MNRAS, 512, 5339
Rosas-Guevara, Y., Bonoli, S., Puchwein, E., Dotti, M., & Contreras, S. 2025, A&A, 698, A20
Springel, V., White, S. D. M., Tormen, G., & Kauffmann, G. 2001, MNRAS, 328, 726
Springel, V., Pakmor, R., Pillepich, A., et al. 2018, MNRAS, 475, 676
Tawfeek, A. A., Cervantes Sodi, B., Fritz, J., et al. 2022, ApJ, 940, 1
Thompson, L. A. 1981, ApJ, 244, L43
Tremaine, S., & Weinberg, M. D. 1984, ApJ, 282, L5
Zhao, D., Du, M., Ho, L. C., Debattista, V. P., & Shi, J. 2020, ApJ, 904, 170
Zhou, Z.-B., Zhu, W., Wang, Y., & Feng, L.-L. 2020, ApJ, 895, 92